# Detection of Left Ventricular Contours Based on Elliptic Approximation and ML Estimate in Angiographic Images

Kyong-Sik Om and Jae-Ho Chung

## Abstract

The goal of this research is to provide a practical algorithm for outlining the left ventricular cavity in digital subtraction angiography. The proposed algorithm is based on the elliptic approximation and ML (Maximum Likelihood) estimate, and it produces a good results regarding execution time, robustness against noise, accuracy, and range of position of ROI (Regions Of Interest).

## I. Introduction

The remarkable development of signal processing technique and computer helps to replace the past passive and subjective analysis of left ventricular image to active and objective one. A well-established method for the assessment of cardiac function in man is the quantitative appraisal of information contained in heart chamber angiography. In particular, the left ventricle (LV) deserves greater attention because it is a powerful blood pump for the systemic circulation [1] [2] [3].

Most of the work has been directed towards the automatic assessment of functional aspects like *ejection fraction* or *wall motion*. For any of these purposes, the automatic determination of the ventricle boundary is a necessary first step. The algorithms that have been proposed up to now have many shortcomings - regarding execution time, robustness against noise, accuracy, and the limit of the position of ROI (Regions Of Interest). The algorithm proposed in this paper overcomes these problems, and it has possibility to be run on practical analysis of LV at clinic.

This paper is organized as follows. In Section II our algorithm is depicted in detail. Section III contains experimental results. Finally, in Section IV conclusions are stated.

Manuscript received July 20, 1995; accepted May 21, 1996.

K. S. Om is with Department of Biomedical Engineering, Seoul National University, Seoul, Korea.

J. H. Chung is with Department of Electronic Engineering, Inha University, Inchon, Korea.

## II. Detection of Left Ventricular Contours

The early study in the literature adopted the heuristic search method which is so empirical that the performance cannot be satisfied [1]. So transformed coordinates were introduced such as long axis method (LAM) [4] and polar coordinate [2] [5]. A popular system is the polar coordinate which is one-dimensional scalar descriptions of the contours. But this coordinate cannot describe highly pathological cases and systolic phase. Also, in this system, the center of LV must be near to center of image.

Thus, we propose another coordinate which is based on elliptic approximation and has insensitivity to phase and position of LV in DSA (Digital Subtraction Angiography).

### *1. Proposed coordinate for LV analysis*

Our proposed coordinate for LV analysis is depicted in Fig. 1. Between the two focal points the slice is perpendicular to the line which crosses the two focal points, and out of these points the coordinate is equal to polar coordinate. So the determination of two focal points is the remained problem in this coordinate. The LV resembles the ellipse but not exactly the same. Consequently, rough positioning of the focal points does not cause problem. Here we set focal points $F1$ and $F2$ such as stated in Equations (2) and (3).

$$C = \frac{1}{2}\{ V1 + V2 \} \quad (1)$$

$$F1 = \frac{1}{3}\{ C + A \} \quad (2)$$

$$F2 = \frac{2}{3}\{ C + A \} \quad (3)$$

The focal points are the basic driving centers in the one-dimensional scalar descriptions of the contours.

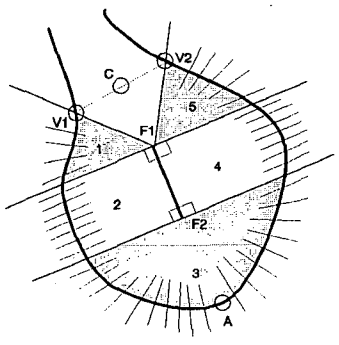


*V1* : Valve point 1 (input point)
*V2* : Valve point 2 (input point)
*A* : Apex (input point)
C : Center point between V1 and V2
*F1*, *F2* : Focal points 1, 2.

**Fig. 1.** Proposed coordinate for LV analysis.

*2. ML estimator*

In radiographic image there are three main sources of noise : quantum noise, scattered radiation and thermal noise. We can regard these random perturbations as being AWGN (additive white Gaussian noise) with variance $\sigma^2$ dependent on the image intensity [6] [7].

From Bayes law the *a posteriori* probability of the contour is

$$P(r \mid I) = \frac{P(I \mid r)P(r)}{P(I)}, \quad (4)$$

where $P(r)$ is the *a priori* probability of the contour $r$, and $P(I \mid r)$ is the conditional probability of the observed image $I$, given the contour.

We set the $I$ such that

$$I=\{I(S_i, h); i\in\{1,2,\cdots,M\}, h\in\{1,2,\cdots,2R+1\}\}, \quad (5)$$

where $S_i$ and $h$ denote step in ellipse coordinate and distance in considering range, respectively.

For the sake of algorithmic simplicity, the image intensity function $I_0$ is assumed as follows.

$$I_0(S_i, h, r_i)=\begin{cases} A_i+n & \text{for } h<r_i \\ B_i+n & \text{for } h>r_i \end{cases} \quad (6)$$

In Eqn. (6), $n$ is noise sequences with variance $\sigma^2$. It is assumed that $A_i > B_i$ and $A_i$ corresponds to LV and $B_i$ to background. Image intensity function $I_0$ is shown in Fig. 2.

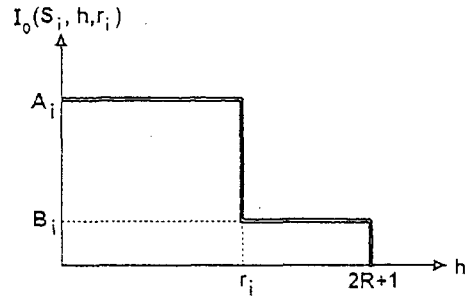


**Fig. 2.** Image intensity function $I_0(S_i, h, r_i)$.

Let's define two new vectors $f_i$ and $g_i$ such as

$$f_i = [\, I_0(S_i,1,r_i), I_0(S_i,2,r_i), \cdots, I_0(S_i,2R+1,r_i)\,]^T$$
$$g_i = [\, I(S_i,1,r_i), I(S_i,2,r_i), \cdots, I(S_i,2R+1,r_i)\,]^T \quad (7)$$

Then, the likelihood function $P(g_i \mid r_i)$ can be written as

$$P(g_i \mid r_i)=\frac{1}{(\sqrt{2\pi})^{2R+1}} \cdot \frac{1}{\sigma^{2R+1}} \cdot \exp\left\{-\frac{1}{2\sigma^2}\,[f_i-g_i]^T\,[f_i-g_i]\right\} \quad (8)$$

Note that $P(g_i \mid r_i)$ depends on $r_i$ through vector $f_i$. Introducing Eqn. (6) into Eqn. (8) the log-likelihood function $L$ becomes

$$L=\ln(P(g_i \mid r_i)) \propto \frac{1}{\sigma^2}\,[2V_i^T g_i - r_i(A_i^2-B_i^2) - g_i^T g_i]\,, \quad (9)$$

where $\propto$ means proportionality and $V_i$ is a vector of dimension $2R+1$ given by

$$V_i = [\, A_i, A_i, \cdots, A_i, B_i, B_i, \cdots, B_i\,], \quad (10)$$

where the number of $A_i$ is $r_i$ and the number of $B_i$ is $2R-r_i$.

The variance $\sigma^2$ can be estimated such as Eqn. (11) where $x_n$ means the observed signals [8].

$$\hat{\sigma}^2=\frac{1}{N}\sum_{i=1}^{N} x_n^2\,. \quad (11)$$

However, from the Eqn. (9), since $\sigma^2$ is only a scale factor and $g_i^T g_i$ is a constant, we can see that log-likelihood function $L$ can be expressed as,

$$L' = 2V_i^T g_i - r_i(A_i^2-B_i^2). \quad (12)$$

We can get $A_i$ (LV level) and $B_i$ (Background level) as in Equations (13) and (14), where $R$ is a *half width of range of ML estimator* (see Fig. 2.).

$$A_i = \frac{1}{R/2}\sum_{j=1}^{R/2} g_i[j] \quad (13)$$

$$B_i = \frac{1}{R/2}\sum_{j=R+1+R/2}^{2R+1} g_i[j] \quad (14)$$

Since the boundary point between LV and background is not exact $R$+1 in Equations (13) and (14), the range of $j$ is shortened.

The *threshold for dynamic range* $r_t$ , then, is compared with the difference between $S$ and $B$, i.e.,

$$r_i = A_i - B_i. \tag{15}$$

If $r_i < r_t$ the tracking process stops. This occurs when the dye is not spread well so the image is too bad to be analyzed. This parameter is used to identify the condition that density of the X-ray contrast material along the LV is approaching the background level.

*3. Tracking position and direction of ML estimator*

Let's consider Fig. 3. Here the $K$th *boundary point* $\mathbf{P}_K$ and $\mathbf{P}_{K+d}$ can be expressed as stated in Eqn. (16) where $d$ is a *look-ahead distance* [pixels].

$$\tilde{\mathbf{P}}_{K+d} = \mathbf{P}_K + d \cdot \hat{\mathbf{U}}_K. \tag{16}$$

For Fig. 3(a), we can observe the followings.

$$\mathbf{U} = \frac{\mathbf{P}_K - \mathbf{C}}{\| \mathbf{P}_K - \mathbf{C} \|} \tag{17}$$

$$\mathbf{P}_{K+d} = \begin{bmatrix} P_K^x + d \cdot U_y \\ P_K^y - d \cdot U_x \end{bmatrix} \tag{18}$$

where $\mathbf{U}$ means the unit direction vector. The $i$th element in the density profile vector $g_{K+d}[\,i\,]$ is given by

$$g_{K+d}[\,i\,] = GL - 1 - G[\,P_{K+d}^x + (i-R-1)\cdot U_x,\ P_{K+d}^y + (i-R-1)\cdot U_y\,] \tag{19}$$

where $G[\,\cdot\,,\,\cdot\,]$ denotes the gray-scale value and $GL$ means the gray level. Here the reason that $g_{K+d}[\,i\,]$ is not equal to $G[\,\cdot\,,\,\cdot\,]$ stems from the assumption that DSA image is negative.

Also, from Fig. 3(b), we get

$$\mathbf{U} = \frac{\mathbf{C}_2 - \mathbf{C}_1}{\| \mathbf{C}_2 - \mathbf{C}_1 \|} \tag{20}$$

$$\mathbf{P}_{K+d} = \begin{bmatrix} P_K^x + d \cdot U_x \\ P_K^y + d \cdot U_y \end{bmatrix} \tag{21}$$

$$g_{K+d}[\,i\,] = GL - 1 - G[\,P_{K+d}^x + (i-R-1)\cdot U_y,\ P_{K+d}^y + (i-R-1)\cdot U_x\,] \tag{22}$$

where $\mathbf{C}_1$ and $\mathbf{C}_2$ correspond to $F1$ and $F2$ for region 2, and to $F2$ and $F1$ for region 4, respectively, in Fig. 1.

After getting array of $g[\ ]$, the ML function is processed and $\mathbf{P}_{K+d}$ is updated. Our extrapolation-update process of tracking is illustrated geometrically in Fig. 3.

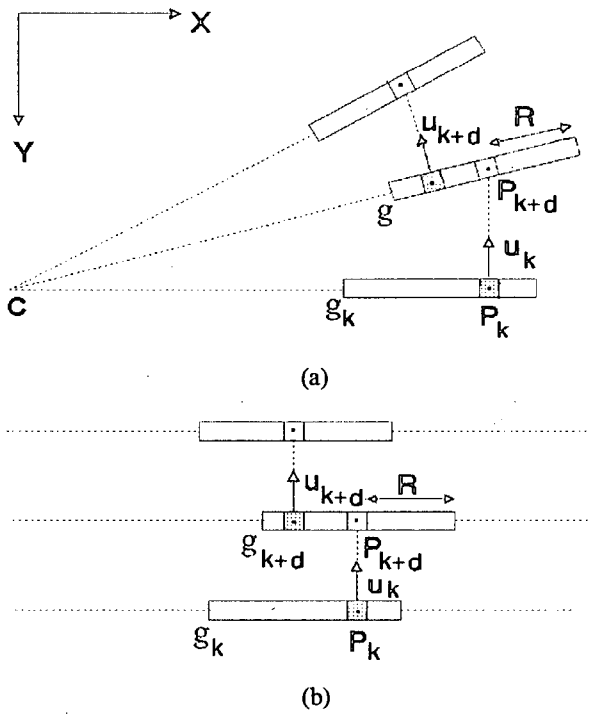


**Fig. 3.** Geometric Illustration of the extrapolation -update process of tracking.
(a) For region of 1, 3, 5 in Fig. 1.
(b) For region of 2, 4 in Fig. 1.

*4. Spatial averaging*

After getting array of $\mathbf{P}_K$, we apply average filter to it. Sandor *et al.* [9] [10] suggested that, if properly implemented, averaging adjacent scan profiles can enhance the precision of the vessel diameter measurements. This concept also can be applied to our algorithm as Eqn. (23) where $l$ is the *half length of average filter*, i.e.,

$$\bar{\mathbf{P}}_K = \frac{1}{2l+1} \sum_{i=-l}^{l} \mathbf{P}_{K+i} \tag{23}$$

This low-pass digital filter does not introduce any spatial phase shift due to its symmetrical structure. This filter is used to explore the subpixel resolution in the measurements based on the assumption of spatial continuity.

## III. Experimental results

First of all, we evaluate the performance of $L'$ in Eqn. (12). Even if the noise variance is large, the performance of ML estimate is good and can find the boundary very well as shown in Fig. 4. These examples show the robustness of our proposed algorithm against the noise when compared to what would be obtained with a local edge detection operator. Especially, even if there is an abrupt change as in Fig. 4(c),

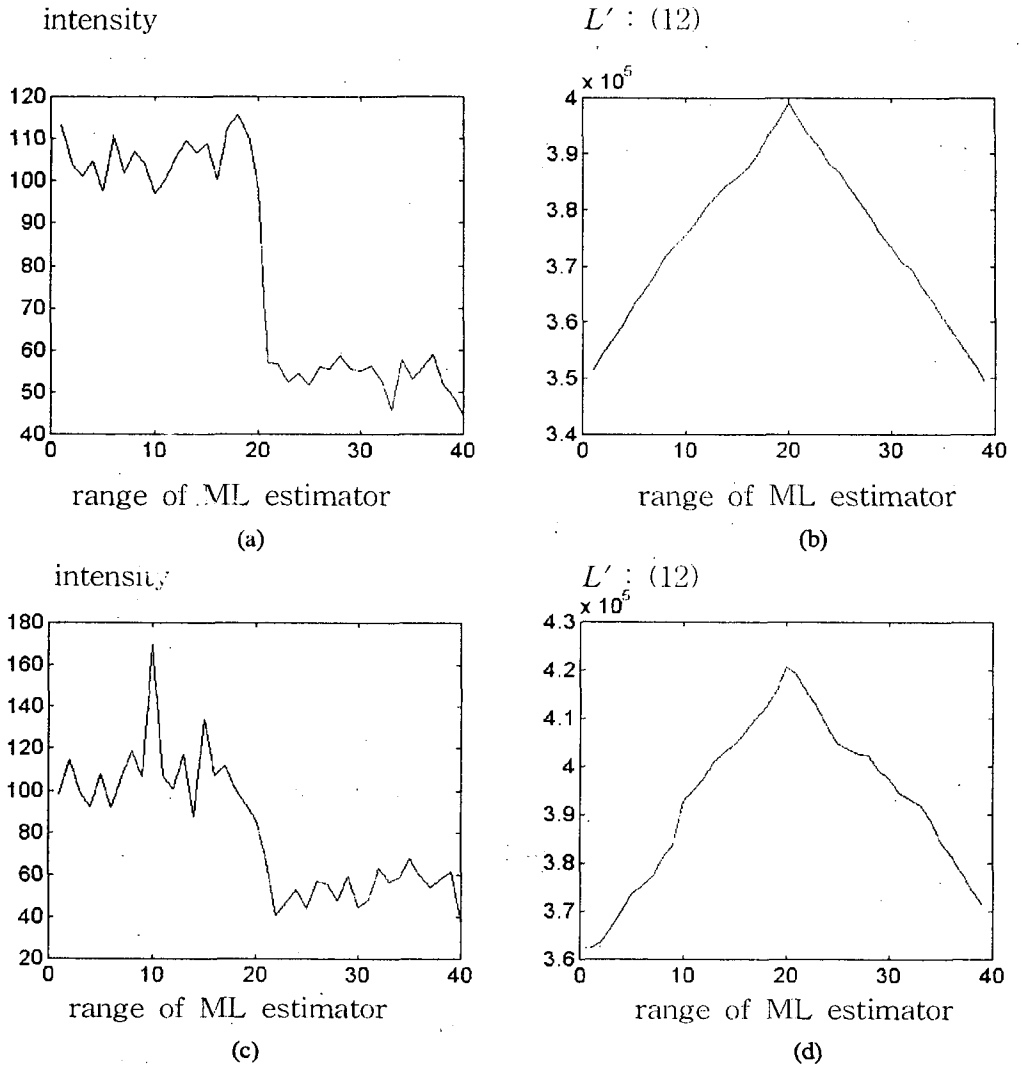


**Fig. 4.** (a) Ideal step edge ($A$=105, $B$=55, boundary point=20) with AWGN ($\sigma$=5).
(b) ML value L' of (a).
(c) Ideal step edge ($A$=105, $B$=55, boundary point=20) with AWGN ($\sigma$=10) and impulse (magnitude=170, position=10).

the corresponding ML estimates are not influenced very well and there is only a very weak local maximum at its location as shown in Fig. 4(d).

We have tested out algorithm at synthetic and real DSA image data with spatial resolution of 512 × 512 and 256 gray levels. The used parameters are $\{r_t, d, R, l\}$={5, 5, 20, 2}. The algorithm was implemented using C-language and tested on IBM compatible 486 PC DX2 50.

Fig. 5 shows that our algorithm is robust against noise ($\sigma$ = 25 is a very high deviation considering the difference between LV and background intensity is 50). Especially, Fig. 5(c) tells us that the final average filtering is efficient compared with Fig. 5(b).

Fig. 6 is the results for real DSA data. Our algorithm can find the LV boundary satisfactorily. Above all, Fig. 6(b) reveals that our algorithm has wide range of position of ROI.

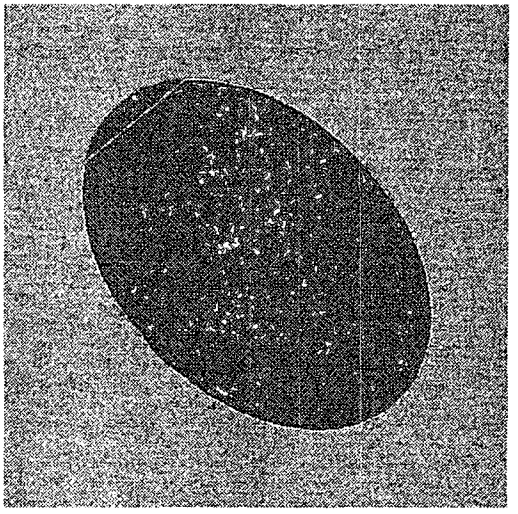

(a)

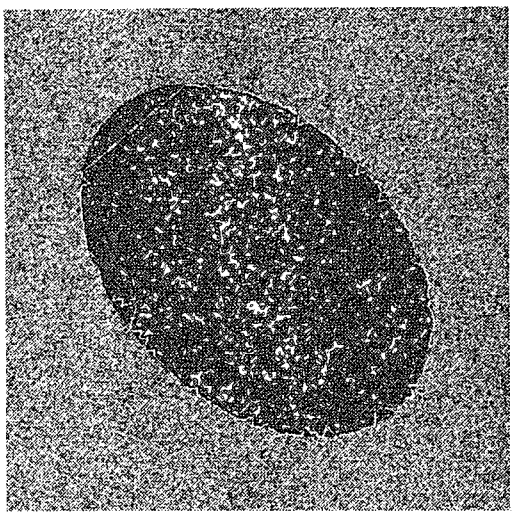

(b)

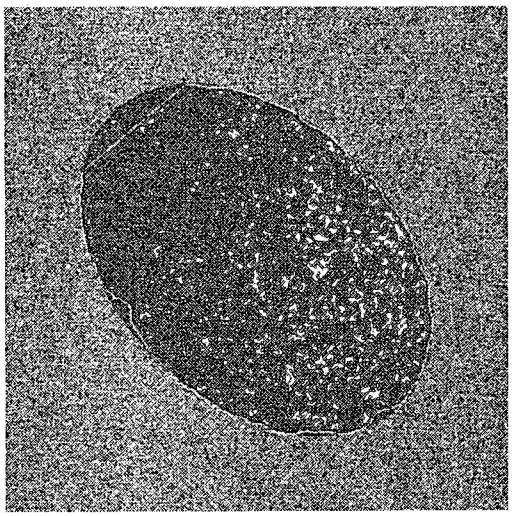

(c)

**Fig. 5.** Synthetic image (ellipse intensity=100, background intensity=150) corrupted by AWGN.
(a) standard deviation $\sigma$=10.
(b) standard deviation $\sigma$=25 and without average filtering.
(c) standard deviation $\sigma$=25 and with average filtering.

Notice that this image cannot be applied to previous polar coordinate which requires that the position of ROI should be near to center of image [2] [5].

The execution time is influenced by parameters. Under previous parameters ( $\{r_t, d, R, l\}=\{5, 5, 20, 2\}$ ), the execution time is about 2 (sec) excluding the time for operator's specification of the valve points 1, 2, and apex. This is a very fast performance compared with previous algorithms, e.g., method of [2] takes about 100 (sec) which uses dynamic programming techniques and method of [5] takes about 20 (sec) which uses Bayesian estimation and Markov random fields, and both methods [2] [5] use full range of polar coordinate.

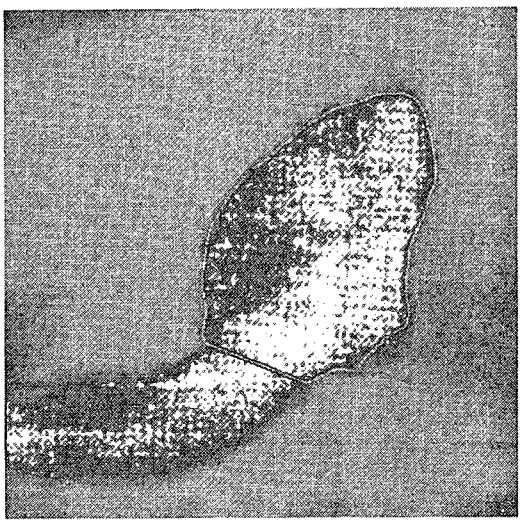

(a)

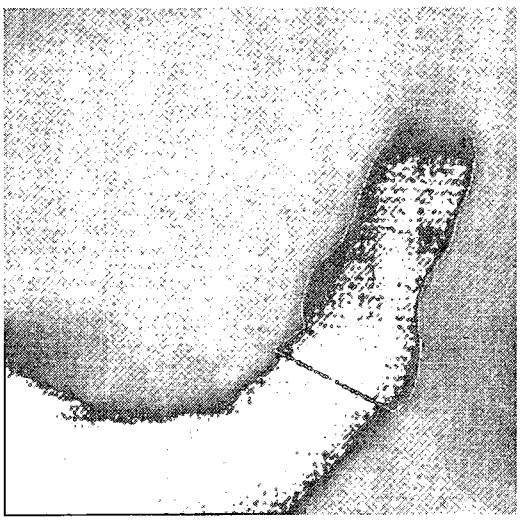

(b)

**Fig. 6.** Real DSA images.
(a) diastolic phase.
(b) systolic phase.

## IV. Conclusions

We have proposed a new algorithm for detecting the left ventricular contours. We have shown by the computer simulation results that our algorithm produces a good results regarding execution time, robustness against noise, accuracy, and range of position of ROI. Especially, considering the execution time our algorithm has shown the possibility to be

run at clinic in practice. We can say that our algorithm is based on elliptic approximation and ML estimate.

Future study can be concentrated on the fully automatic detection of LV contours. This could be accomplished by using the concept of artificial intelligence.

## References


[1] P. Grattoni and R. Bonamini, "Contour Detection of the Left Ventricular Cavity from Angiographic Images," *IEEE Trans. Medical Imaging*, Vol. MI-4, No.2, June, 1985.

[2] B. H. Koo, T. S. Lee, K. S. Park, B. G. Min, M. C. Han and J. H. Park, "A Measurement of Heart Ejection Fraction Using Automatic Detection of Left Ventricular Boundary in Digital Angiocardiogram," *J. of KOSOMBE*, Vol. 8, No. 2, pp. 177-188, 1987.

[3] J. S. Duncan, F. A. Lee and A. W. M. Smeulders, "A Bending Energy Model for Measurement of Cardiac Shape Deformity," *IEEE Trans. Medical Imaging*, Vol. 10, No. 1, September, 1991.

[4] E. Marcus, P. Lorents, E. Bartha, R. Beyar, D. Adam, and S. Sideman, "A comparative study of quantitative methods for characterization of left ventricular contraction," in *Proc. Comput. Cardiol.*, pp. 145-148, 1985.

[5] M. T. de Figueiredo, "Bayesian Estimation of Ventricular Contours in Angiographic Images," *IEEE Trans. Medical Imaging*, Vol. 11, No. 3, September, 1992.

[6] R. Kruger, "X-ray digital cineangiography," in *Cardiac Imaging and Image process*, S. Collins and D. Skorton, Eds. McGraw-Hill, New York, pp. 206-238, 1986.

[7] J. Reiber, P. Serruys, and C. Slager, *Quantitative Coronary and left Ventricular Cineangiography*, Dordrecht, The Netherlands: Martinus- Nijhoff Publishers, 1986.

[8] J. Teuber, *Digital Image Processing*, Prentice Hall, 1993.

[9] T. Sandor, A. D'Adamo, W. B. Hanlon, and J. R. Spears, "High precision quantitative angiography," *IEEE Trans. Medical Imaging*, Vol. MI-6, pp. 258-265, 1987.

[10] Y. Sun, "Automated Identification of Vessel Contours in Coronary Arteriograms by an Adaptive Tracking Algorithm," *IEEE Trans. Medical Imaging*, Vol. 8, No. 1, pp. 78-88, March, 1989.


**Kyong-Sik Om** was born in Korea, in 1971. He received the B.S. and M.S. degrees in electronic engineering from Inha University, Inchon, Korea, in 1994 and 1996, respectively. Since 1996, he has been working toward the Ph.D degree in Biomedical Engineering at Seoul National University, Seoul, Korea. His research interests include artificial organs, intelligent control, biological signal and image processing. He is a student member of KITE, KOSOMBE, ICASE, KFIS.

**Jae-Ho Chung** was received the B.S. and M.S. degrees in Electrical Engineering from University of Maryland, and the Ph.D. degree in Electrical Engineering from Georgia Institute of Technology, in 1982, 1984, and 1990, respectively. During 1984～1985, he was an electronic engineer at Naval Surface Warfare Center, U.S.A. During 1991～1992, he worked as a member of technical staff at AT&T Bell Laboratories, U.S.A. He joined the Department of Electronic Engineering at Inha University in 1992 as an Assistant Professor, where he is currently an Associate Professor.